Available online at www.sciencedirect.com
ScienceDirect
Journal of Sound and Vibration 323 (2009) 772–789
JOURNAL OF SOUND AND VIBRATION
www.elsevier.com/locate/jsvi

Studies on dynamic behavior of functionally graded cylindrical shells with PZT layers under moving loads

G.G. Sheng[a,b], X. Wang[a,*]

[a]*School of Naval Architecture, Ocean and Civil Engineering (State Key Laboratory of Ocean Engineering), Shanghai Jiaotong University, Shanghai 200240, People's Republic of China*
[b]*School of Civil Engineering and Architecture, Changsha University of Science and Technology, Changsha, Hunan 410076, People's Republic of China*

Received 14 October 2008; received in revised form 5 January 2009; accepted 8 January 2009
Handling Editor: L.G. Tham
Available online 3 March 2009

Abstract

Based on the first-order shear deformation theory (FSDT), the Hamilton's principle and the Maxwell equation, this paper presents the coupling equations to govern the electric potential and the displacements of the functionally graded cylindrical shell with surface-bonded PZT piezoelectric layer, and subjected to moving loads. The frequencies equations are obtained by using displacement functions and one electric potential function. The modal analysis technique and Newmark's integration method are used to calculate the displacements and sensory electric potential of the shell subjected to moving loads. The effects of the moving velocities of the loads, volume fraction exponents Φ of functionally graded materials (FGMs) and temperature environment on the dynamic responses of shells are investigated. An analytical approximate equation is obtained to describe the relationship between critical velocities of moving loads and natural frequencies of shells. The present approach is validated by comparing the natural frequencies with the result presented by Ng et al. In addition, numerical results show the relationship between the displacements and sensory electric potential of the shell. The present work shows that some meaningful and interesting results presented in this paper are helpful for the application and the design of smart sensory structures.

1. Introduction

Smart structures, consisting of piezoelectric materials integrated with structural systems, have been an important research object since many years due to their unique feature to couple electric and mechanical characteristics. In recent years, the development of integration of piezoelectric materials to the composite structures is paid special attentions to their potential applications of aerospace and aircraft structures, civil structures, marine and automobiles which require intelligent functions [1,2]. A smart structure that contains the main structure and the distributed piezoelectric sensor/actuators can sense the excitations induced by its environment and can also generate control forces to eliminate the undesirable effects or to enhance the

*Corresponding author.
E-mail addresses: jeffery710@163.com (G.G. Sheng), xwang@sjtu.edu.cn (X. Wang).

0022-460X/$ - see front matter © 2009 Elsevier Ltd. All rights reserved.
doi:10.1016/j.jsv.2009.01.017

desirable effects. Yang et al. [3] developed a generic electromechanical impedance model for the two-dimensional PZT—structure interaction systems. To closely simulate the real situation, the PZT transducers were assumed to interact with the host structure at four edges. The results for a plate structure were in good agreement with the experimental measurements. Yang and Hu [4] presented an electromechanical impedance model for health monitoring of cylindrical shell structures. By investigating the interaction between the PZT transducers and a typical cylindrical shell structure, the electromechanical impedance of the PZT transducers is obtained. Several analytical and finite element studies have been presented for hybrid beams and plates with thickness poled actuators [5,6]. D'Ottavio et al. [7] solved the free-vibration problem of multilayered shells with embedded piezoelectric materials. Closed-form solutions are given for the free-vibration problem of simply supported, orthotropic piezoelectric laminates. The formulations are applied to study the influence of the electromechanical coupling on the resonant frequencies. Vel et al. [8] presented an analytical solution for the static deformation and steady-state vibration of simply supported hybrid cylindrical shells consisting of fiber-reinforced layers with embedded piezoelectric shear sensors and actuators. Suitable displacement and electric potential functions that identically satisfy the boundary conditions at the simply supported edges are used to reduce the governing equations of static deformation and steady-state vibrations. Besides, temperature variation can bring about voltage or charge generation in piezoelectric sensors [9], which is referred to as pyroelectric effect. Tzou et al. [10] found from their numerical studies that temperature variation considerably influences the electric potential distribution on both piezoelectric sensor and actuator layers.

Due to the advantages of being able to withstand severe high-temperature gradient while maintaining structural integrity, functionally graded materials (FGMs) have been receiving much more attention in engineering communities, especially in applications for high-temperature environment [11,12]. Some researchers have developed various approximated theories and computation methods for FGM structures. The extension of the unified formulation (UF) to FGM structures was provided in Refs. [13,14]. Comparisons with three-dimensional solutions confirmed the efficiency of the extension of UF to FGM structures analysis, even for very thick structures.

Piezoelectric FGM structures will have the advantages of FGMs and piezoelectric materials linked together. Hybrid piezoelectric FGM structures are one type of FGM piezoelectric structures, where a substrate made of FGMs is integrated with surface-bonded piezoelectric actuator and/or sensor layers.

Mirzavand and Eslami [15] presented a thermal buckling analysis for functionally graded cylindrical shells that are integrated with surface-bonded piezoelectric actuators and are subjected to the combined action of thermal load and constant applied actuator voltage. He et al. [16] studied the vibration control of the FGM plates with integrated piezoelectric sensors and actuators by a finite element formulation based on the classical laminated plate theory. Ng et al. [17], Liew et al. [18,19] have explored the application of piezoelectric sensor–actuator for active control of vibration of FGMs structural members both under ambient conditions as well as varying temperature environment.

Dynamical problems of beams, plates and cylindrical shells subjected to an action of moving loads already have a long history in mechanics [20–25]. A moving load causes the radial displacements of an axi-symmetric shell to be several times higher than that produced by the static application of the same load [26]. On the other hand, the moving sources (e.g., heat fluid-conveying, impacting waves, the moving of heat field and work pieces during machining operations etc.) will often occur in the rocket, aircraft, nuclear vessels and chemical pipes, as well as the industry of shipbuilding.

In this study, the deformation of FGM shells with piezoelectric layers is to satisfy the limitation of first-order shear deformation theory (FSDT), in which material properties of FGM are considered as graded across the shell thickness according to a power-law, in terms of the volume fractions of the constituents. For the piezoelectric layer, temperature distribution is linear across its thickness, and for the FGM layer, temperature distribution is nonlinear. The Hamilton's principle, the Maxwell equation and the FSDT considering rotary and in-plane inertias have been utilized to model the dynamics characteristic of FGM cylindrical shells with surface-bonded PZT piezoelectric layers, and subjected to moving loads. By using the modal analysis technique and Newmark's integration method, a better approximation is obtained, and a faster convergence method is achieved for the dynamic responses of FGM cylindrical shells subjected to moving loads. Finally, the natural frequencies from the present method are compared with those results found in the open literature, and a good comparison is obtained between the results.

2. Theoretical formulations

An FGM cylindrical shell with mean radius of R and the length L is shown in Fig. 1. A deformable piezoelectric layer is perfectly bonded on its outer surface as sensor. The z-axis is the thickness coordinate for both piezoelectric layer and FGM layer. The thickness of the FGM layer is denoted by h and that of the piezoelectric layer is h_P. The piezoelectric layer is polarized along the thickness direction. The displacement components in the x, θ and z directions are denoted by u, v and w, respectively.

The material properties of FGM cylindrical shells are accurately modeled, by using a simple rule of mixtures. The volume fraction is described by a spatial function as follows:

$$\Psi(z) = \left(\frac{z + h/2}{h}\right)^{\Phi} \quad (0 \leqslant \Phi \leqslant \infty) \tag{1}$$

where Φ expresses the volume fraction exponent. The combination of these functions gives rise to the effective properties of FGMs [11]. The temperature change referenced to the stress free state (the room temperature T_0) is considered as

$$\Delta T(x, \theta, z, t) = \Gamma(x, \theta, t) T(z)$$

The stress resultants of the FGM layer are given by

$$\begin{Bmatrix} N_x \\ N_\theta \\ N_{x\theta} \\ M_x \\ M_\theta \\ M_{x\theta} \end{Bmatrix} = \begin{bmatrix} A_{11} & A_{12} & 0 & B_{11} & B_{12} & 0 \\ A_{21} & A_{22} & 0 & B_{21} & B_{22} & 0 \\ 0 & 0 & A_{66} & 0 & 0 & B_{66} \\ B_{11} & B_{12} & 0 & D_{11} & D_{12} & 0 \\ B_{21} & B_{22} & 0 & D_{21} & D_{22} & 0 \\ 0 & 0 & B_{66} & 0 & 0 & D_{66} \end{bmatrix} \begin{Bmatrix} \varepsilon_x \\ \varepsilon_\theta \\ \gamma_{x\theta} \\ \kappa_x \\ \kappa_\theta \\ \kappa_{x\theta} \end{Bmatrix} - \begin{Bmatrix} N_x^T \\ N_\theta^T \\ N_{x\theta}^T \\ M_x^T \\ M_\theta^T \\ M_{x\theta}^T \end{Bmatrix} \tag{2}$$

$$\begin{Bmatrix} Q_x \\ Q_\theta \end{Bmatrix} = \begin{bmatrix} C_{44} & 0 \\ 0 & C_{55} \end{bmatrix} \begin{Bmatrix} \gamma_{xz} \\ \gamma_{\theta z} \end{Bmatrix} \tag{3}$$

where

$$(A_{ij}, B_{ij}, D_{ij}) = \int_{-h/2}^{h/2} Q_{ij}(1, z, z^2)\,\mathrm{d}z \quad (i,j = 1,2,6), \quad C_{44} = \int_{-h/2}^{h/2} Q_{55}\,\mathrm{d}z, \quad C_{55} = \int_{-h/2}^{h/2} Q_{44}\,\mathrm{d}z,$$

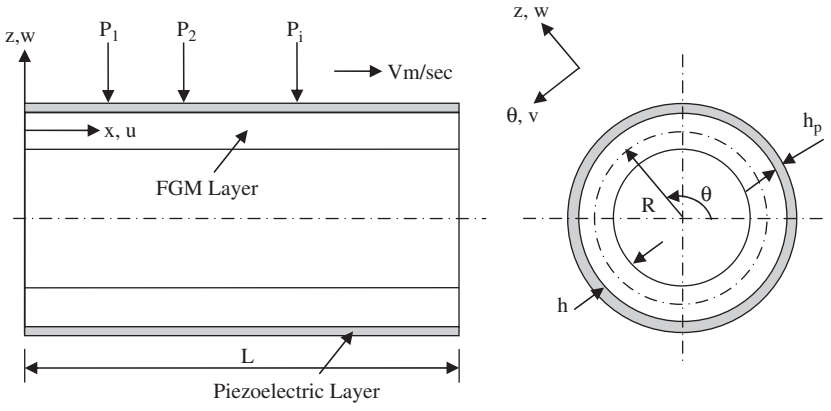

Fig. 1. Coordinate system of the FGM cylindrical shell with surface-bonded PZT layer under moving loads.

$$\begin{Bmatrix} N_x^T & M_x^T \\ N_\theta^T & M_\theta^T \\ N_{x\theta}^T & M_{x\theta}^T \end{Bmatrix} = \Gamma(x,\theta,t)\int_{-h/2}^{h/2} \begin{Bmatrix} (Q_{11}(z)+Q_{12}(z))\alpha_{eff}(z) \\ (Q_{12}(z)+Q_{22}(z))\alpha_{eff}(z) \\ 0 \end{Bmatrix} (1 \;\; z) T(z)\,\mathrm{d}z$$

where the effective elasticity coefficients $Q_{ij}(z)$ and thermal expansion coefficients $\alpha_{eff}(z)$ of the FGM layer are given by Kadoli and Ganesan [27]. ε_x, ε_θ, $\gamma_{x\theta}$, γ_{xz} and $\gamma_{\theta z}$ is the mid-surface strains of the FGM layer, κ_x, κ_θ and $\kappa_{x\theta}$ is the mid-surface curvatures.

According to the state of generalized plane stress of the thin shell assumption [28], the constitutive equations of piezoelectric layer can be expressed by the direct and the converse piezoelectric equations, respectively.

$$\begin{Bmatrix} \sigma_x^P \\ \sigma_\theta^P \\ \tau_{x\theta}^P \\ \tau_{\theta z}^P \\ \tau_{xz}^P \end{Bmatrix} = \begin{bmatrix} Q_{11e} & Q_{12e} & 0 & 0 & 0 \\ Q_{12e} & Q_{22e} & 0 & 0 & 0 \\ 0 & 0 & Q_{66e} & 0 & 0 \\ 0 & 0 & 0 & Q_{44e} & 0 \\ 0 & 0 & 0 & 0 & Q_{55e} \end{bmatrix} \begin{Bmatrix} \bar{\varepsilon}_x - \alpha_{11e}\Delta T \\ \bar{\varepsilon}_\theta - \alpha_{22e}\Delta T \\ \bar{\gamma}_{x\theta} \\ \bar{\gamma}_{\theta z} \\ \bar{\gamma}_{xz} \end{Bmatrix} - \begin{bmatrix} 0 & 0 & e_{31e} \\ 0 & 0 & e_{32e} \\ 0 & 0 & 0 \\ 0 & e_{24e} & 0 \\ e_{15e} & 0 & 0 \end{bmatrix} \begin{Bmatrix} E_x \\ E_\theta \\ E_z \end{Bmatrix} \tag{4}$$

$$\begin{Bmatrix} D_x \\ D_\theta \\ D_z \end{Bmatrix} = \begin{bmatrix} 0 & 0 & 0 & e_{15e} & 0 \\ 0 & 0 & e_{24e} & 0 & 0 \\ e_{31e} & e_{32e} & 0 & 0 & 0 \end{bmatrix} \begin{Bmatrix} \bar{\varepsilon}_x \\ \bar{\varepsilon}_\theta \\ \bar{\gamma}_{\theta z} \\ \bar{\gamma}_{xz} \\ \bar{\gamma}_{x\theta} \end{Bmatrix} + \begin{bmatrix} \xi_{11e} & 0 & 0 \\ 0 & \xi_{22e} & 0 \\ 0 & 0 & \xi_{33e} \end{bmatrix} \begin{Bmatrix} E_x \\ E_\theta \\ E_z \end{Bmatrix} + \Delta T \begin{Bmatrix} p_{xe} \\ p_{\theta e} \\ p_{ze} \end{Bmatrix} \tag{5}$$

Effective constants of the piezoelectric layer are given by

$$Q_{11e} = Q_{11}^P - \frac{Q_{13}^P Q_{13}^P}{Q_{33}^P}, \quad Q_{12e} = Q_{12}^P - \frac{Q_{13}Q_{23}}{Q_{33}}$$

$$Q_{22e} = Q_{22}^P - \frac{Q_{23}^P Q_{23}^P}{Q_{33}^P}, \quad Q_{44e} = Q_{44}^P, \quad Q_{55e} = Q_{55}^P, \quad Q_{66e} = Q_{66}^P$$

$$\alpha_{11e} = \alpha_{11} - \frac{Q_{13}^P}{Q_{33}^P}(Q_{31}^P\alpha_{11} + Q_{32}^P\alpha_{22}), \quad \alpha_{22e} = \alpha_{22} - \frac{Q_{23}^P}{Q_{33}^P}(Q_{31}^P\alpha_{11} + Q_{32}^P\alpha_{22})$$

$$e_{31e} = e_{31} - \frac{Q_{13}^P}{Q_{33}^P}e_{33}, \quad e_{32e} = e_{32} - \frac{Q_{23}^P}{Q_{33}^P}e_{33}, \quad e_{15e} = e_{15}, \quad e_{24e} = e_{24}, \quad \xi_{11e} = \xi_{11}$$

$$\xi_{22e} = \xi_{22}, \quad \xi_{33e} = \xi_{33} + \frac{e_{33}^2}{Q_{33}^E}, \quad p_{xe} = p_x, \quad p_{\theta e} = p_\theta$$

$$p_{ze} = p_z + \frac{e_{33}}{Q_{33}^P}(Q_{31}^P\alpha_{11} + Q_{32}^P\alpha_{22} + Q_{33}^P\alpha_{33})$$

where $\bar{\varepsilon}_x$, $\bar{\varepsilon}_\theta$, $\bar{\gamma}_{x\theta}$, $\bar{\gamma}_{xz}$ and $\bar{\gamma}_{\theta z}$ is the strains of an arbitrary point in the piezoelectric layer, and σ_x^P, σ_θ^P, $\tau_{x\theta}^P$, $\tau_{\theta z}^P$ and τ_{xz}^P is the corresponding stresses. $\{D_x \;\; D_\theta \;\; D_z\}^T$, $\{E_x \;\; E_\theta \;\; E_z\}^T$ and $\{p_x \;\; p_\theta \;\; p_z\}^T$ represent the electric displacements, electric fields and pyroelectric constants of the piezoelectric layer, respectively. Q_{ij}^P, e_{ij}, ξ_{ij} and α_{ij} denote the elastic constants, piezoelectric constants, dielectric constants and thermal expansion coefficients, respectively.

In the above formula, the electric fields are expressed as a function of the electric potential φ in the curvilinear coordinate system as follows:

$$E_x = -\frac{\partial \varphi}{\partial x}, \quad E_\theta = -\frac{1}{R+z}\frac{\partial \varphi}{\partial \theta}, \quad E_z = -\frac{\partial \varphi}{\partial z} \tag{6}$$

The piezoelectric layer considered in this paper take as a sensor and the electric potential is induced by elastic deformation in the piezoelectric layer. The distribution of electric potential in the piezoelectric layer is given by [29]

$$\varphi(x,\theta,z,t) = P(z_P)\psi(x,\theta,t) \tag{7}$$

z_P is the local thickness coordinate with respect to the piezoelectric layer mid-plane, $z_P = z - z_0$, $z_0 = (h+h_P)/2$. The function $P(z_P)$ is defined by

$$P(z_P) = z_P^2 - \left(\frac{h_P}{2}\right)^2 \tag{8}$$

The strains of an arbitrary point $\bar{\varepsilon}_x$, $\bar{\varepsilon}_\theta$, $\bar{\gamma}_{x\theta}$, $\bar{\gamma}_{xz}$ and $\bar{\gamma}_{\theta z}$ in Eqs. (4) and (5) are related to the mid-surface strains and curvatures of the FGM layer [27]. The stress resultants of piezoelectric layer are computed using Eq. (4) as follows:

$$\begin{Bmatrix} N_x^P \\ N_\theta^P \\ N_{x\theta}^P \\ M_x^P \\ M_\theta^P \\ M_{x\theta}^P \end{Bmatrix} = \begin{bmatrix} A_{11}^P & A_{12}^P & 0 & B_{11}^P & B_{12}^P & 0 \\ A_{21}^P & A_{22}^P & 0 & B_{21}^P & B_{22}^P & 0 \\ 0 & 0 & A_{66}^P & 0 & 0 & B_{66}^P \\ B_{11}^P & B_{12}^P & 0 & D_{11}^P & D_{12}^P & 0 \\ B_{21}^P & B_{22}^P & 0 & D_{21}^P & D_{22}^P & 0 \\ 0 & 0 & B_{66}^P & 0 & 0 & D_{66}^P \end{bmatrix} \begin{Bmatrix} \varepsilon_x \\ \varepsilon_\theta \\ \gamma_{x\theta} \\ \kappa_x \\ \kappa_\theta \\ \kappa_{x\theta} \end{Bmatrix} - \begin{Bmatrix} N_x^{PT} \\ N_\theta^{PT} \\ N_{x\theta}^{PT} \\ M_x^{PT} \\ M_\theta^{PT} \\ M_{x\theta}^{PT} \end{Bmatrix} + \begin{Bmatrix} N_x^E \\ N_\theta^E \\ N_{x\theta}^E \\ M_x^E \\ M_\theta^E \\ M_{x\theta}^E \end{Bmatrix} \tag{9}$$

$$\begin{Bmatrix} Q_x^P \\ Q_\theta^P \end{Bmatrix} = \begin{bmatrix} C_{44}^P & 0 \\ 0 & C_{55}^P \end{bmatrix} \begin{Bmatrix} \gamma_{xz} \\ \gamma_{\theta z} \end{Bmatrix} + \begin{Bmatrix} Q_x^E \\ Q_\theta^E \end{Bmatrix} \tag{10}$$

$$(A_{ij}^P, B_{ij}^P, D_{ij}^P) = \int_{h/2}^{h/2+h_P} Q_{ije}(1, z, z^2)\,\mathrm{d}z \quad (i,j = 1,2,6)$$

$$C_{44}^P = \int_{h/2}^{h/2+h_P} Q_{55e}\,\mathrm{d}z, \quad C_{55}^P = \int_{h/2}^{h/2+h_P} Q_{44e}\,\mathrm{d}z$$

where the thermal force resultants of the piezoelectric layer are defined as follows:

$$\begin{Bmatrix} N_x^{PT} & M_x^{PT} \\ N_\theta^{PT} & M_\theta^{PT} \\ N_{x\theta}^{PT} & M_{x\theta}^{PT} \end{Bmatrix} = \Gamma(x,\theta,t) \int_{h/2}^{h/2+h_P} \begin{Bmatrix} (Q_{11e}\alpha_{11e} + Q_{12e}\alpha_{22e}) \\ (Q_{12e}\alpha_{11e} + Q_{22e}\alpha_{22e}) \\ 0 \end{Bmatrix} (1 \;\; z) T(z)\,\mathrm{d}z$$

The piezoelectric resultants of the piezoelectric layer are defined as follows:

$$\begin{Bmatrix} N_x^E \\ N_\theta^E \\ N_{x\theta}^E \end{Bmatrix} = \begin{Bmatrix} 2e_{31e}\int_{h/2}^{h/2+h_P} z_P\,\mathrm{d}z \\ 2e_{32e}\int_{h/2}^{h/2+h_P} z_P\,\mathrm{d}z \\ 0 \end{Bmatrix} \psi, \quad \begin{Bmatrix} M_x^E \\ M_\theta^E \\ M_{x\theta}^E \end{Bmatrix} = \begin{Bmatrix} 2e_{31e}\int_{h/2}^{h/2+h_P} z_P z\,\mathrm{d}z \\ 2e_{32e}\int_{h/2}^{h/2+h_P} z_P z\,\mathrm{d}z \\ 0 \end{Bmatrix} \psi$$

$$Q_x^E = e_{15}\int_{h/2}^{h/2+h_P} P(z_P)\,\mathrm{d}z \frac{\partial \psi}{\partial x}, \quad Q_\theta^E = e_{24}\int_{h/2}^{h/2+h_P} \frac{P(z_P)}{R+z}\,\mathrm{d}z \frac{\partial \psi}{\partial \theta}$$

As shown in Fig. 1, a row of loads $P_i(t)\,(i=1,2,\ldots,N_P)$ move along the longitudinal axis at constant speed V. The load function $p(x,t)$ describing the action on the shell is expressed as [30]

$$p(x,t)=\sum_{i=1}^{N_P}P_i(t)\delta(x-x_i)\delta(\theta-\theta_0)U_i(t) \tag{11}$$

where

$$U_i(t)=H_1(t-t_{i-1})[1-H_2(t-t_{i-1}-t_L)]$$

$$x_i=V(t-t_{i-1})\quad(0\leqslant x_i\leqslant L),\quad t_L=L/V$$

$\delta(.)$ denotes Dirac delta function, $H_i(t)\,(i=1,2)$ denotes Heaviside unit step function, (x_i,θ_0) denotes the location of the moving load $P_i(t)$ at time t, and t_{i-1} denotes arriving time of the i-th load at the shell. The corresponding work of the moving loads can be expressed as [24]

$$W_P=\int_A p(x,t)w(x,\theta,t)R\,\mathrm{d}\theta\,\mathrm{d}x \tag{12}$$

The potential energy V_{N_0} of the axial loading (N_0) is taken as [31]

$$V_{N_0}=\frac{1}{2}\int_A\left[N_0\left(\frac{\partial w}{\partial x}\right)^2+N_0\left(\frac{\partial v}{\partial x}\right)^2\right]R\,\mathrm{d}\theta\,\mathrm{d}x \tag{13}$$

For thin shells, as are the cases used here, the transversal displacement is assumed to be constant through the thickness. Based on the FSDT and Hamilton's principle, the equations of motion for an FGM cylindrical shell with surface-bonded piezoelectric layer under axially load N_0 and moving loads are as follows [28]:

$$\frac{\partial(N_x+N_x^P)}{\partial x}+\frac{1}{R}\frac{\partial(N_{x\theta}+N_{x\theta}^P)}{\partial\theta}=(I_1+I_1^P)\ddot{u}+(I_2+I_2^P)\ddot{\phi}_x$$

$$\frac{1}{R}\frac{\partial(N_\theta+N_\theta^P)}{\partial\theta}+\frac{\partial(N_{x\theta}+N_{x\theta}^P)}{\partial x}+\frac{1}{R}(Q_\theta+Q_\theta^P)+N_0\frac{\partial^2 v}{\partial x^2}=(I_1+I_1^P)\ddot{v}+(I_2+I_2^P)\ddot{\phi}_\theta$$

$$\frac{1}{R}\frac{\partial(Q_\theta+Q_\theta^P)}{\partial\theta}+\frac{\partial(Q_x+Q_x^P)}{\partial x}-\frac{1}{R}(N_\theta+N_\theta^P)+N_0\frac{\partial^2 w}{\partial x^2}+p(x,t)=(I_1+I_1^P)\ddot{w}$$

$$\frac{\partial(M_x+M_x^P)}{\partial x}+\frac{1}{R}\frac{\partial(M_{x\theta}+M_{x\theta}^P)}{\partial\theta}-(Q_x+Q_x^P)=(I_2+I_2^P)\ddot{u}+(I_3+I_3^P)\ddot{\phi}_x$$

$$\frac{1}{R}\frac{\partial(M_\theta+M_\theta^P)}{\partial\theta}+\frac{\partial(M_{x\theta}+M_{x\theta}^P)}{\partial x}-(Q_\theta+Q_\theta^P)=(I_2+I_2^P)\ddot{v}+(I_3+I_3^P)\ddot{\phi}_\theta \tag{14}$$

where ϕ_x and ϕ_θ are the slope in-plane of x–z and θ–z, respectively. The strains, curvature expressions and mass terms of Eqs. (2), (3), (9), (10) and (14) are defined as

$$\varepsilon_x=\frac{\partial u}{\partial x},\quad \varepsilon_\theta=\frac{1}{R}\left(\frac{\partial v}{\partial\theta}+w\right),\quad \gamma_{x\theta}=\frac{\partial v}{\partial x}+\frac{1}{R}\frac{\partial u}{\partial\theta},\quad \gamma_{xz}=\phi_x+\frac{\partial w}{\partial x},\quad \gamma_{\theta z}=\phi_\theta+\frac{1}{R}\frac{\partial w}{\partial\theta}$$

$$\kappa_x=\frac{\partial\phi_x}{\partial x},\quad \kappa_\theta=\frac{1}{R}\frac{\partial\phi_\theta}{\partial\theta},\quad \kappa_{x\theta}=\frac{\partial\phi_\theta}{\partial x}+\frac{1}{R}\frac{\partial\phi_x}{\partial\theta} \tag{15}$$

$$(I_1,I_2,I_3)=\int_{-h/2}^{h/2}\rho_{eff}(z)(1,z,z^2)\,\mathrm{d}z,\quad (I_1^P,I_2^P,I_3^P)=\int_{h/2}^{h/2+h_P}\rho^P(1,z,z^2)\,\mathrm{d}z \tag{16}$$

$\rho_{eff}(z)$ is the effective mass density of the FGM layer, and ρ^P is the mass density of the piezoelectric layer.

Utilizing Eqs. (2), (3), (9), (10) and (15), the equations of motion can be expressed in terms of generalized displacement $(u, v, w, \phi_x, \phi_\theta)$ as follows:

$$
\begin{aligned}
&L_{11}u + L_{12}v + L_{13}w + L_{14}\phi_x + L_{15}\phi_\theta + L_{16}\psi + a_1\Gamma'_x = (I_1 + I_1^P)\ddot{u} + (I_2 + I_2^P)\ddot{\phi}_x\\
&L_{21}u + L_{22}v + L_{23}w + L_{24}\phi_x + L_{25}\phi_\theta + L_{26}\psi + N_0\frac{\partial^2 v}{\partial x^2} + a_2\Gamma'_\theta = (I_1 + I_1^P)\ddot{v} + (I_2 + I_2^P)\ddot{\phi}_\theta\\
&L_{31}u + L_{32}v + L_{33}w + L_{34}\phi_x + L_{35}\phi_\theta + L_{36}\psi + N_0\frac{\partial^2 w}{\partial x^2} + a_3\Gamma + p(x,t) = (I_1 + I_1^P)\ddot{w}\\
&L_{41}u + L_{42}v + L_{43}w + L_{44}\phi_x + L_{45}\phi_\theta + L_{46}\psi + a_4\Gamma'_x = (I_2 + I_2^P)\ddot{u} + (I_3 + I_3^P)\ddot{\phi}_x\\
&L_{51}u + L_{52}v + L_{53}w + L_{54}\phi_x + L_{55}\phi_\theta + L_{56}\psi + a_5\Gamma'_\theta = (I_2 + I_2^P)\ddot{v} + (I_3 + I_3^P)\ddot{\phi}_\theta
\end{aligned}
\tag{17}
$$

The Maxwell equation [8] is

$$
\int_{h/2}^{h/2+h_P}\left(\frac{\partial D_x}{\partial x} + \frac{1}{R}\frac{\partial D_\theta}{\partial \theta} + \frac{\partial D_z}{\partial z} + \frac{1}{R}D_z\right)\mathrm{d}z = 0 \tag{18}
$$

Utilizing Eq. (5), the charge equilibrium Eq. (18) can be expressed as follows:

$$
L_{61}u + L_{62}v + L_{63}w + L_{64}\phi_x + L_{65}\phi_\theta + L_{66}\psi = a_{61}\Gamma'_x + a_{62}\Gamma'_\theta + a_{63}\Gamma \tag{19}
$$

where L_{ij} $(i,j = 1, 2, \ldots, 6)$ and some coefficients in Eqs. (17) and (19) are defined in Appendix A.

Here, the two ends of the FGM cylindrical shell with surface-bonded piezoelectric layer are considered as simply supported, so that a solution for the motion Eqs. (17) and the charge equilibrium Eq. (19) can be described by

$$
\begin{aligned}
&u = \sum_{m=0}^{M}\sum_{n=0}^{N} u_{mn}(t)\cos\lambda_m x\cos n\theta, \quad v = \sum_{m=1}^{M}\sum_{n=1}^{N} v_{mn}(t)\sin\lambda_m x\sin n\theta\\
&w = \sum_{m=1}^{M}\sum_{n=0}^{N} w_{mn}(t)\sin\lambda_m x\cos n\theta, \quad \phi_x = \sum_{m=0}^{M}\sum_{n=0}^{N} \phi_{mn}(t)\cos\lambda_m x\cos n\theta\\
&\phi_\theta = \sum_{m=1}^{M}\sum_{n=1}^{N} \bar{\phi}_{mn}(t)\sin\lambda_m x\sin n\theta, \quad \psi = \sum_{m=1}^{M}\sum_{n=0}^{N} \psi_{mn}(t)\sin\lambda_m x\cos n\theta
\end{aligned}
\tag{20}
$$

where $\lambda_m = m\pi/L$, n represents the number of circumferential waves and m represents the number of axial half-waves.

The generalized forces related to the thermal load in Eqs. (17) and (19) can also be expanded in double Fourier series

$$
\begin{aligned}
&a_1\Gamma'_x = \sum_{m=0}^{M}\sum_{n=0}^{N} q_{mn1}(t)\cos\lambda_m x\cos n\theta, \quad a_2\Gamma'_\theta = \sum_{m=1}^{M}\sum_{n=1}^{N} q_{mn2}(t)\sin\lambda_m x\sin n\theta\\
&a_3\Gamma = \sum_{m=1}^{M}\sum_{n=0}^{N} q_{mn3}(t)\sin\lambda_m x\cos n\theta, \quad a_4\Gamma'_x = \sum_{m=0}^{M}\sum_{n=0}^{N} q_{mn4}(t)\cos\lambda_m x\cos n\theta\\
&a_5\Gamma'_\theta = \sum_{m=1}^{M}\sum_{n=1}^{N} q_{mn5}(t)\sin\lambda_m x\sin n\theta, \quad a_{61}\Gamma'_x + a_{62}\Gamma'_\theta + a_{63}\Gamma = \sum_{m=1}^{M}\sum_{n=0}^{N} q_{mn6}(t)\sin\lambda_m x\cos n\theta
\end{aligned}
\tag{21}
$$

Substituting Eqs. (20) and (21) into Eqs. (17) and (19), yields:

$$
\begin{aligned}
&(I_1 + I_1^E)\ddot{u}_{mn}(t) + (I_2 + I_2^E)\ddot{\phi}_{mn}(t) + T_{11}u_{mn}(t) + T_{12}v_{mn}(t)\\
&\quad + T_{13}w_{mn}(t) + T_{14}\phi_{mn}(t) + T_{15}\bar{\phi}_{mn}(t) + T_{16}\psi_{mn}(t) = q_{mn1}(t)
\end{aligned}
\tag{22}
$$

$$
\begin{aligned}
&(I_1 + I_1^E)\ddot{v}_{mn}(t) + (I_2 + I_2^E)\ddot{\bar{\phi}}_{mn}(t) + T_{21}u_{mn}(t) + [T_{22} + \lambda_m^2 N_0]v_{mn}(t)\\
&\quad + T_{23}w_{mn}(t) + T_{24}\phi_{mn}(t) + T_{25}\bar{\phi}_{mn}(t) + T_{26}\psi_{mn}(t) = q_{mn2}(t)
\end{aligned}
\tag{23}
$$

$$(I_1 + I_1^E)\ddot{w}_{mn}(t) + T_{31}u_{mn}(t) + T_{32}v_{mn}(t) + [T_{33} + \lambda_m^2 N_0]w_{mn}(t) + T_{34}\phi_{mn}(t) + T_{35}\bar{\phi}_{mn}(t) + T_{36}\psi_{mn}(t) = q_{mn3}(t) + \frac{2}{\pi L}\sum_{i=1}^{N_P} P_i(t)\sin\lambda_m x_i(t)\cos n\theta_0 \tag{24}$$

$$(I_2 + I_2^E)\ddot{u}_{mn}(t) + (I_3 + I_3^E)\ddot{\bar{\phi}}_{mn}(t) + T_{41}u_{mn}(t) + T_{42}v_{mn}(t) + T_{43}w_{mn}(t) + T_{44}\phi_{mn}(t) + T_{45}\bar{\phi}_{mn}(t) + T_{46}\psi_{mn}(t) = q_{mn4}(t) \tag{25}$$

$$(I_2 + I_2^E)\ddot{v}_{mn}(t) + (I_3 + I_3^E)\ddot{\bar{\phi}}_{mn}(t) + T_{51}u_{mn}(t) + T_{52}v_{mn}(t) + T_{53}w_{mn}(t) + T_{54}\phi_{mn}(t) + T_{55}\bar{\phi}_{mn}(t) + T_{56}\psi_{mn}(t) = q_{mn5}(t) \tag{26}$$

$$T_{61}u_{mn}(t) + T_{62}v_{mn}(t) + T_{63}w_{mn}(t) + T_{64}\phi_{mn}(t) + T_{65}\bar{\phi}_{mn}(t) + T_{66}\psi_{mn}(t) = q_{mn6}(t) \tag{27}$$

where the unknown constants T_{ij} can be determined by operators L_{ij} in Eqs. (17) and (19).

From the Eq. (27), the induced electric potential coefficient $\psi_{mn}(t)$ is obtained as follows:

$$\psi_{mn}(t) = \frac{1}{T_{66}}[q_{mn6}(t) - T_{61}u_{mn}(t) - T_{62}v_{mn}(t) - T_{63}w_{mn}(t) - T_{64}\phi_{mn}(t)) - T_{65}\bar{\phi}_{mn}(t)] \tag{28}$$

Substituting Eq. (28) into Eqs. (22)–(26), the following governing equations are obtained:

$$[M]\{\ddot{q}\} + \left([K_E] - \frac{1}{T_{66}}\{K_{P1}\}\{K_{P2}\}^T\right)\{q\} = \{F_M\} + \{F_T\} + \{F_{TP}\} \tag{29}$$

where

$$[M] = \begin{bmatrix} I_1 + I_1^P & 0 & 0 & I_2 + I_2^P & 0 \\ 0 & I_1 + I_1^P & 0 & 0 & I_2 + I_2^P \\ 0 & 0 & I_1 + I_1^P & 0 & 0 \\ I_2 + I_2^P & 0 & 0 & I_3 + I_3^P & 0 \\ 0 & I_2 + I_2^P & 0 & 0 & I_3 + I_3^P \end{bmatrix}$$

$$[K_E] = \begin{bmatrix} T_{11} & T_{12} & T_{13} & T_{14} & T_{15} \\ T_{21} & T_{22} + \lambda_m^2 N_0 & T_{23} & T_{24} & T_{25} \\ T_{31} & T_{32} & T_{33} + \lambda_m^2 N_0 & T_{34} & T_{35} \\ T_{41} & T_{42} & T_{43} & T_{44} & T_{45} \\ T_{51} & T_{52} & T_{53} & T_{54} & T_{55} \end{bmatrix}$$

$$\{K_{P1}\}^T = \{T_{16}\ \ T_{26}\ \ T_{36}\ \ T_{46}\ \ T_{56}\}, \quad \{K_{P2}\}^T = \{T_{61}\ \ T_{62}\ \ T_{63}\ \ T_{64}\ \ T_{65}\}$$

$$\{q\} = \{u_{mn}\ \ v_{mn}\ \ \phi_{mn}\ \ \bar{\phi}_{mn}\}^T$$

$$\{F_M\}^T = \left\{0\ \ 0\ \ \frac{2}{\pi L}\sum_{i=1}^{N_P} P_i(t)\sin\lambda_m x_i(t)\cos n\theta_0\ \ 0\ \ 0\right\}$$

$$\{F_T\}^T = \{q_{mn1}(t)\ \ q_{mn2}(t)\ \ q_{mn3}(t)\ \ q_{mn4}(t)\ \ q_{mn5}(t)\}$$

$$\{F_{TP}\} = -\frac{1}{T_{66}}\{K_{P1}\}q_{mn6}(t)$$

$\{F_M\}^T$, $\{F_T\}^T$ and $\{F_{TP}\}$ are the generalized forces related to the moving loads, the thermal load and the thermo-piezoelectric coupling, respectively.

We set $\{F\} = \{F_M\} + \{F_T\} + \{F_{TP}\} = 0$, and substitute

$$u_{mn}(t) = u_{mn}^0 e^{i\omega t}, \quad v_{mn}(t) = v_{mn}^0 e^{i\omega t}, \quad w_{mn}(t) = w_{mn}^0 e^{i\omega t}, \ldots$$

into Eq. (29) and obtain the following 5×5 system of eigenvalue problem:

$$([K] - \omega^2[M])\{\Delta\} = \{0\} \tag{30}$$

where $\{\Delta\}^T = \{u_{mn}^0 \ v_{mn}^0 \ w_{mn}^0 \ \phi_{mn}^0 \ \bar{\phi}_{mn}^0\}$, the nontrivial solution of the eigen-equation (30) gives the natural frequencies of the FGM cylindrical shell with surface-bonded piezoelectric layer.

3. Numerical results and discussions

The magnitudes of the moving loads in this paper are identical ($P_i(t) = P_0 = \text{constant}$). The generalized forces related to the moving loads, the thermal load and the thermopiezoelectric coupling are expressed as

$$\{F_M\}^T = \left\{ 0 \ \ 0 \ \ \frac{2P_0}{\pi L} \sum_{i=1}^{N_P} \sin \lambda_m x_i(t) \cos n\theta_0 \ \ 0 \ \ 0 \right\}$$

$$\{F_T\}^T = \begin{cases} \left\{ 0 \ \ 0 \ \ \dfrac{4a_3}{\pi m}[1 - (-1)^m]\Gamma(t) \ \ 0 \ \ 0 \right\} & n = 0 \\ \{0 \ \ 0 \ \ 0 \ \ 0 \ \ 0\} & n \neq 0 \end{cases}$$

$$\{F_{TP}\} = -\frac{1}{T_{66}}\{K_{P1}\}q_{mn6}(t) = \begin{cases} -\dfrac{1}{T_{66}}\{K_{P1}\}\dfrac{4a_{63}}{\pi m}[1 - (-1)^m]\Gamma(t) & n = 0 \\ 0 & n \neq 0 \end{cases}$$

In this study, in-plane uniform distribution of temperature is considered as

$$\Gamma(x, \theta, t) = \Gamma(t) \quad (\Delta T(x, \theta, z, t) = T(z)\Gamma(t)) \tag{31}$$

The temperature distribution along the thickness of the shell can be obtained by solving a steady-state heat transfer equation [32]. For the piezoelectric layer, temperature distribution across the thickness is considered as linear:

$$T(z) = T_m + \frac{T_0 - T_m}{h_P}\left(z - \frac{h}{2}\right) - T_0 \quad \left(\frac{h}{2} \leqslant z \leqslant \frac{h}{2} + h_P\right) \tag{32}$$

and for the FGM layer:

$$T(z) = T_c - \frac{T_c - T_m}{\int_{-h/2}^{h/2} dz/k_{eff}(z)} \int_{-h/2}^{z} \frac{dz}{k_{eff}(z)} - T_0 \quad \left(-\frac{h}{2} \leqslant z \leqslant \frac{h}{2}\right) \tag{33}$$

where T_c, T_m are the temperature of the inner surface and the outer surface of the FGM layer, respectively. k_{eff} is the effective thermal conductivity of the FGM layer. T_0 is the room temperature (zero thermal stress state, $T_0 = 300\,\text{K}$). T_m can be obtained by utilizing the temperature continuous conditions between the FGM layer and piezoelectric layer, and the heat transfer equation. The temperature difference between the inner surface and the outer surface of the shell is $T_{c0} = T_c - T_0$.

The ceramic and the metal materials of the functionally graded layer in this study are considered as zirconia and aluminum [28]. The properties for the two materials are listed as

Aluminum

$$E_m = 70\,\text{GPa}, \quad v_m = 0.3, \quad \rho_m = 2707\,\text{kg/m}^3, \quad k_m = 204\,\text{W/mK}, \quad \alpha_m = 23 \times 10^{-6}\,^\circ\text{C}$$

Zirconia

$$E_c = 151\,\text{GPa}, \quad v_c = 0.3, \quad \rho_c = 3000\,\text{kg/m}^3, \quad k_c = 2.09\,\text{W/mK}, \quad \alpha_c = 10 \times 10^{-6}\,^\circ\text{C}$$

The piezoelectric layer is made of PZT-4. The material constants are given by Ramirez et al. [33] and Ganesan and Kadoli [34]. The other calculation data are given by

$$R = 1\,\mathrm{m}, \quad h/R = 0.01, \quad h_P/R = 0.001, \quad P_0 = 50\,\mathrm{KN}, \quad \theta_0 = \frac{\pi}{4}, \quad \Gamma(t) = \sin\ 100t.$$

3.1. Free-vibration studies on the FGM shell with surface-bonded piezoelectric layer

Free-vibration natural frequency characteristics are presented for the FGM shell with surface-bonded piezoelectric layer, and the effects of wavenumber and axial compressive load on the free-vibration natural frequencies of the shell are investigated.

For cylindrical shells of intermediate length, as are the cases used here, the buckling load is given by Timoshenko and Gere [35]

$$N_{0cr} = \frac{Eh^2}{R[3(1-\upsilon]^{1/2}} \tag{34}$$

and the axial load can be nondimensionalized as $\bar{N}_0 = N_0/N_{0cr}$, and E, υ are the material constants of Aluminum in Eq. (34). The nondimensional natural frequencies Ω is defined as [36]

$$\Omega^2 = (I_1 R^2/E)\omega^2, \quad E = E_m h/(1-\upsilon_m^2) \tag{35}$$

From Fig. 2, it is seen that as the axial half-waves m ($m \leqslant 4$) increases, the lowest fundamental frequency gets shifted to the right-hand side of the curve. The behavior is similar to conventional shells [36]. When vibration modes (m, n) are (1,1), (2,1), (3,1) and (4,1), the fundamental frequencies are almost same. Moreover, when $m \geqslant 5$, the fundamental frequency of the FGM cylindrical shell with surface-bonded piezoelectric layer increases as the circumferential mode n increases, which are not agreement with those for homogeneous isotropic cylindrical shells presented by Radwan et al. [36].

It is clear from the results in Table 1 that when the ratio of length to radius L/R of the cylindrical shell increases, the fundamental frequency decreases. It can also be observed in Table 1 that the effect of piezoelectric layer on the fundamental frequency is obvious.

3.2. Displacements and sensory response of the shell under moving loads

In this paper, the initial conditions are supposed to be zero, and dynamic responses at the point ($x_1 = L/2$, $\theta_1 = \pi/4$, $z = (h+h_P)/2$) are obtained. Fig. 3 shows convergence of time response $w(x_1, \theta_1, t)$ under a moving

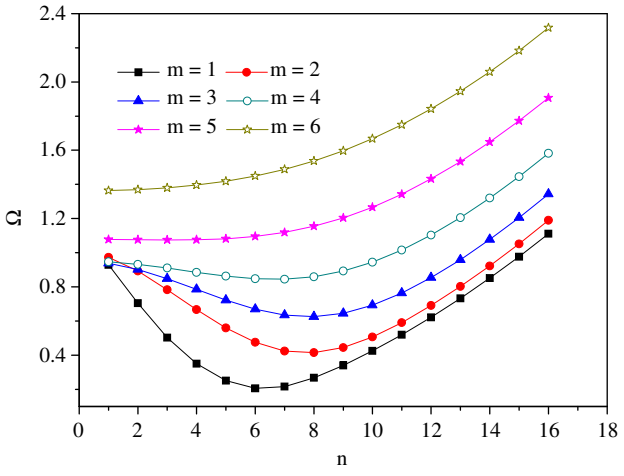

Fig. 2. Nondimensional natural frequency (Ω) versus vibration modes (m, n) for the FGM cylindrical shell with surface-bonded piezoelectric layer ($N_0 = 0.5N_{cr}$, $L/R = 1.0$, $\Phi = 1.0$).

Table 1
Non-dimensional natural frequency Ω versus non-dimensional axial compressive load N_0/N_{cr} for the FGM cylindrical shell with surface-bonded piezoelectric layer ($m = 1$, $n = 1$, $\Phi = 1.0$).

L/R		N_0/N_{cr}				
		0.0	0.2	0.4	0.6	0.8
Elastic effect only	1.0	0.9363	0.9319	0.9276	0.9232	0.9188
Piezoelectric effect		0.9403	0.9359	0.9316	0.9272	0.9228
Elastic effect only	1.1	0.9118	0.9081	0.9044	0.9007	0.8970
Piezoelectric effect		0.9150	0.9114	0.9077	0.9039	0.9002
Elastic effect only	1.2	0.8846	0.8814	0.8782	0.8750	0.8718
Piezoelectric effect		0.8873	0.8841	0.8809	0.8777	0.8745

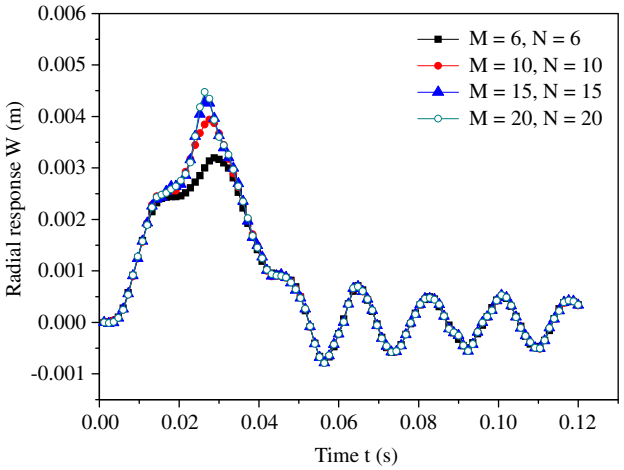

Fig. 3. The convergence of time response $w(x_1, \theta_1, t)$ for various M and N ($L/R = 4.0$, $\Phi = 1.0$, $V = 80\,\mathrm{m/s}$).

load ($N_P = 1$). The time responses are calculated for M,$N = 6$, 10, 15 and 20 in model expansion, respectively. It is concluded that the series (see Eq. (20)) is able to provide a good approximation for the response, and the results using the series converge fast. All the plots are drawn for M,$N = 15$, because the time responses obtained from M,$N = 15$ and 20 in modal expansion are approximately in good agreement.

Many factors have effects on the dynamic responses of the shell subjected to moving loads. The main parameters are the velocities of moving loads, volume fraction exponents Φ of FGMs and temperatures.

To investigate the effect of the velocities of moving loads, a row of loads (the number of moving loads $N_P = 200$) with equal intervals L move along the longitudinal axis at the same moving velocity V. Fig. 4 shows the variation of the maximum dynamic response with the velocity of moving loads. $w_{\max}(x_1, \theta_1, t)$ represents the maximum radial response at the point (x_1, θ_1, z) of the shell as the loads traverse the shell (and also passes this position), while $\varphi_{\max}(x_1, \theta_1, z, t)$ represents the maximum sensory electric potential of the same point. In Fig. 4, the maximum response of the shell shows three predominant peaks, which correspond to the first, the second and the third critical velocities ($V_{cr}^1 = 455\,\mathrm{m/s}$, $V_{cr}^2 = 490\,\mathrm{m/s}$, $V_{cr}^3 = 610\,\mathrm{m/s}$). According to the governing equations (29), the first three critical velocities can also be defined as [20]

$$V_{cr}^i = \frac{\omega_i L}{\pi} \tag{36}$$

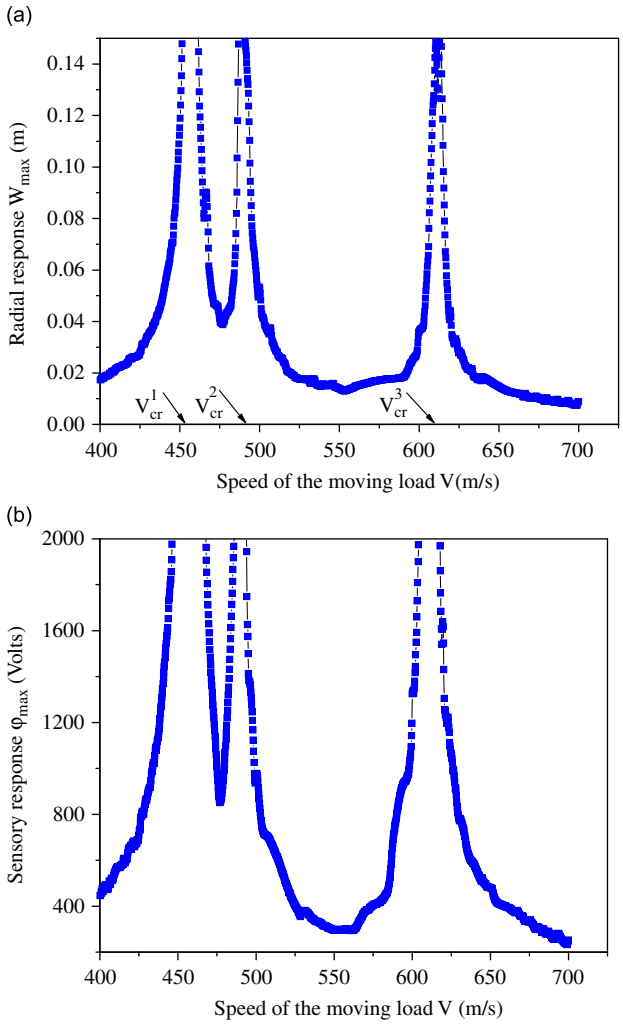

Fig. 4. Maximum transient responses for different moving velocities V: (a) radial response $w_{\max}(x_1, \theta_1, t)$ and (b) sensory electric potential $\varphi_{\max}(x_1, \theta_1, z, t)$ $(L/R = 4.0,\ \Phi = 1.0)$.

where ω_i $(i = 1,2,3)$ is the i-th natural frequency of the shell (see Eq. (30)). The results calculated from Eq. (36) are agreement with the numerical results in Fig. 4. From this study, it is clear that the shell does not have enough time to reach its maximum responses as the speed of moving loads increases and the number N_P of moving loads decreases.

Fig. 5 describes the effect of the material property of the FGM layer on dynamic responses of the shell. It is seen from Fig. 5 that the response amplitude of the shell subjected to a moving load $(N_P = 1)$ decreases with the increases of volume fraction exponent Φ of the FGM layer. But when the volume fraction exponent Φ is larger, such as for $\Phi = 5$ and 10, the results are almost equal. This is due to the fact that the ceramic (zirconia) content in the FGM layer increases as the value of Φ increases, and the elastic modulus of the ceramic, zirconia, is much larger as compared to their metal counterpart (aluminum). The material properties exhibit small variations when the volume fraction exponent Φ is larger, and when $\Phi = \infty$, the FGM layer is fully zirconia. Designers may obtain the desirable dynamic characteristics adequate to design purpose as they choose the volume fraction exponents Φ appropriately. A free vibration can also be observed after the load departs from the shell.

Since the heat flux is applied to the inner surface of the shell, maximum temperature occurs at the inside surface. Fig. 6 shows the radial response and sensory electric potential induced from a moving load and an

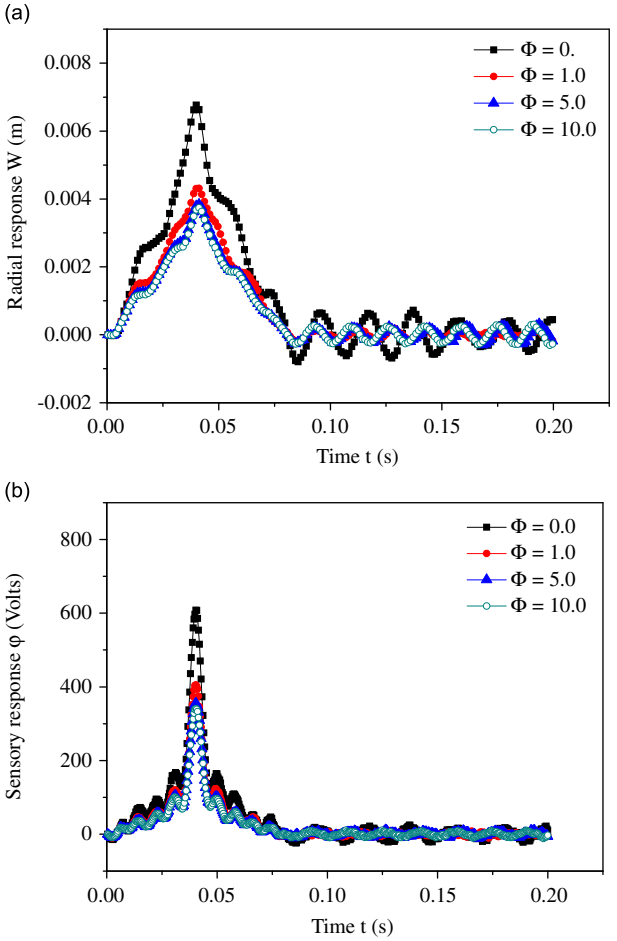

Fig. 5. Influence of different volume fraction exponents Φ on dynamic responses of the shell subjected to a moving load: (a) radial response $w(x_1, \theta_1, t)$ and (b) sensory electric potential $\varphi(x_1, \theta_1, z, t)$ ($L/R = 4.0$, $\Phi = 1.0$, $V = 50$ m/s).

applied thermal load. The temperature differences T_{c0} between the inner surface and the outer surface of the shell are taken as 0, 200, 300 and 400 °C, respectively. As the thermal loading increases, the amplitudes of vibration also increase.

In addition, the radial response and sensory electric potential exhibit the same variation in Figs. 4 and 5. This is due to the fact that temperature effects are not considered in these figures ($q_{mn6}(t) = 0$, see Eq. (28)), and the generalized coordinates $\{u_{mn}(t)\ v_{mn}(t)\ w_{mn}(t)\ \phi_{mn}(t)\ \bar{\phi}_{mn}(t)\}^{\mathrm{T}}$ and induced electric potential coefficient $\psi_{mn}(t)$ exhibit the same variation with time t for the forced vibration. When $q_{mn6}(t) \neq 0$ ($T_{c0} \neq 0$ see Fig. 6), the variation of induced electric potential coefficient $\psi_{mn}(t)$ is not different with that of the generalized coordinates.

3.3. Simple validation of the present method

Because few detailed reports on the dynamic behavior of the FGM cylindrical shell with piezoelectric layer are available in previous literatures, an exact comparison of the present result with existed results is difficult. To verify the present analysis, vibration frequencies of a simple supported silicon nitride-nickel FGM cylindrical shell are computed using the present method (Table 2). The geometric properties are $L/R = 1$ and $R/h = 100$. The nondimensionalized fundamental frequencies P_1 ($P_1 = 4\pi R\omega\sqrt{I_1/A_{11}}$) are compared to those presented by Ng et al. [37]. Excellent agreement in Table 2 is observed with Ng et al.

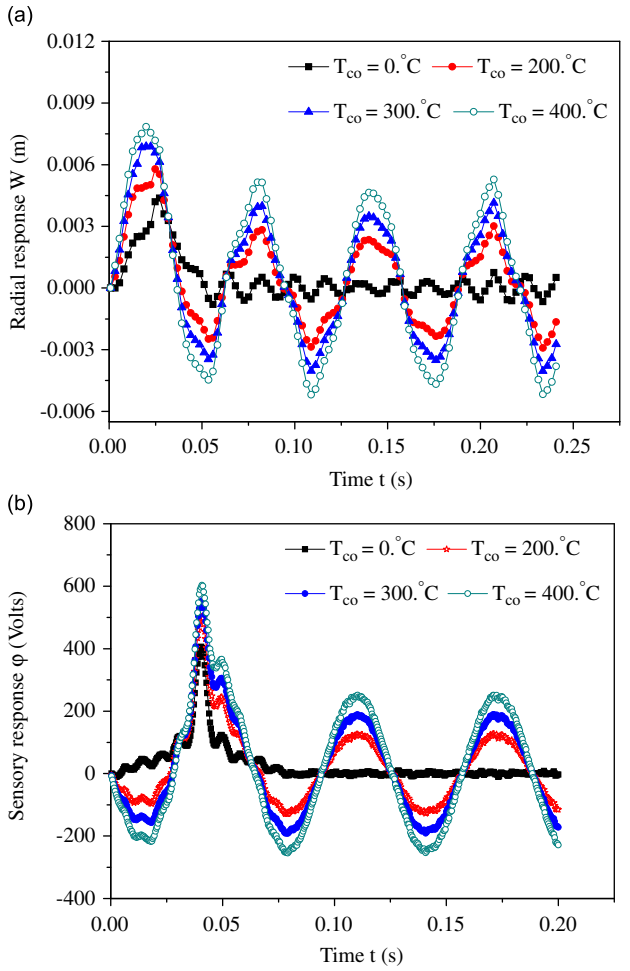

Fig. 6. Influence of different applied thermal loads on dynamic responses of the shell subjected to a moving load: (a) radial response $w(x_1, \theta_1, t)$ and (b) sensory electric potential $\varphi(x_1, \theta_1, z, t)$ ($L/R = 4.0$, $\Phi = 1.0$, $V = 80$ m/s).

Table 2
Comparison of the non-dimensionalized fundamental frequencies P_1 for a simply supported silicon nitride–nickel FGM cylindrical shell subjected to axial compressive loading of $N_0 = 0.5N_{cr}$.

Φ	P_1 (type B) $m = 1$, $n = 1$		P_1 (type B) $m = 1$, $n = 2$	
	Present	Ng et al.	Present	Ng et al.
0	10.371606	10.393196	7.908486	7.9345878
0.5	10.513124	10.526190	8.001219	8.0542139
1.0	10.571836	10.583092	8.083749	8.1037601
5.0	10.662965	10.673575	8.162233	8.1799865
10.0	10.678231	10.689887	8.174746	8.1931948
∞	10.692909	10.707442	8.186364	8.2071402

4. Conclusions

This paper reports the results of an investigation into the dynamics characteristics of FGM cylindrical shells with surface-bonded PZT piezoelectric layer, and under moving loads. Some main consequences are given by

(1) As the axial half-waves m ($m \leqslant 4$) increases, the lowest fundamental frequency occurs at larger circumferential mode n. When $m \geqslant 5$, the fundamental frequency of the FGM cylindrical shell with surface-bonded piezoelectric layer increases as the circumferential mode n increases.
(2) The fundamental frequency of the FGM cylindrical shell with surface-bonded piezoelectric layer decreases as the axial compressive load increases. The piezoelectric effect of piezoelectric layer can increase the fundamental frequency of FGM structures.
(3) The effect of volume fraction exponent of the FGM layer on dynamic responses is obvious only when the volume fraction exponent Φ is less than 5. When the volume fraction exponent Φ is larger than 5, the results are already very close to those associated with $\Phi = \infty$.
(4) The amplitudes of dynamic responses of the shell are significantly influenced by temperature change. As the thermal loading increases, the amplitudes of vibration also increase.

To obtain more accurate results, future research should consider the variation of displacement distributions (not a constant transversal displacement) across the shell thickness [13,14], especially for thick FGM structures.

Acknowledgments

The authors thank the reviewers for their valuable comments and the support of the project: 2006AA09A103.

Appendix A

$$\bar{A}_{ij} = A^P_{ij} + A_{ij}, \quad \bar{B}_{ij} = B^P_{ij} + B_{ij}, \quad \bar{C}_{ij} = C^P_{ij} + C_{ij}, \quad \bar{D}_{ij} = D^P_{ij} + D_{ij}$$

$$L_{11} = \bar{A}_{11}\frac{\partial^2}{\partial x^2} + \frac{1}{R^2}\bar{A}_{66}\frac{\partial^2}{\partial \theta^2}, \quad L_{12} = \frac{\bar{A}_{12} + \bar{A}_{66}}{R}\frac{\partial^2}{\partial x\,\partial \theta}, \quad L_{13} = \frac{\bar{A}_{12}}{R}\frac{\partial}{\partial x}$$

$$L_{14} = \bar{B}_{11}\frac{\partial^2}{\partial x^2} + \frac{\bar{B}_{66}}{R^2}\frac{\partial^2}{\partial \theta^2}, \quad L_{15} = \frac{\bar{B}_{12} + \bar{B}_{66}}{R}\frac{\partial^2}{\partial x\,\partial \theta}, \quad L_{16} = 2e_{31e}\int_{h/2}^{h/2+h_P} z_P\,\mathrm{d}z\frac{\partial}{\partial x}$$

$$L_{21} = \frac{\bar{A}_{66} + \bar{A}_{12}}{R}\frac{\partial^2}{\partial x\,\partial \theta}, \quad L_{22} = \bar{A}_{66}\frac{\partial^2}{\partial x^2} + \frac{\bar{A}_{22}}{R^2}\frac{\partial^2}{\partial \theta^2} - \frac{\bar{C}_{55}}{R^2} + N_0\frac{\partial^2}{\partial x^2}$$

$$L_{23} = \frac{\bar{A}_{22} + \bar{C}_{55}}{R^2}\frac{\partial}{\partial \theta}, \quad L_{24} = \frac{\bar{B}_{66} + \bar{B}_{12}}{R}\frac{\partial^2}{\partial x\,\partial \theta}, \quad L_{25} = \bar{B}_{66}\frac{\partial^2}{\partial x^2} + \frac{\bar{B}_{22}}{R^2}\frac{\partial^2}{\partial \theta^2} + \frac{\bar{C}_{55}}{R}$$

$$L_{26} = \frac{1}{R}\left[e_{24e}\int_{h/2}^{h/2+h_P}\frac{P(z_P)}{R+z}\,\mathrm{d}z + 2e_{32e}\int_{h/2}^{h/2+h_P} z_P\,\mathrm{d}z\right]\frac{\partial}{\partial \theta}, \quad L_{31} = -\frac{\bar{A}_{21}}{R}\frac{\partial}{\partial x}$$

$$L_{32} = -\frac{\bar{C}_{55}}{R^2}\frac{\partial}{\partial \theta} - \frac{\bar{A}_{22}}{R^2}\frac{\partial}{\partial \theta}, \quad L_{33} = \bar{C}_{44}\frac{\partial^2}{\partial x^2} + \frac{\bar{C}_{55}}{R^2}\frac{\partial^2}{\partial \theta^2} - \frac{\bar{A}_{22}}{R^2} + N_0\frac{\partial^2}{\partial x^2}$$

$$L_{34} = \bar{C}_{44}\frac{\partial}{\partial x} - \frac{\bar{B}_{21}}{R}\frac{\partial}{\partial x}, \quad L_{35} = \frac{\bar{C}_{55}}{R}\frac{\partial}{\partial \theta} - \frac{\bar{B}_{22}}{R^2}\frac{\partial}{\partial \theta}$$

$$L_{36} = -\frac{1}{R}2e_{32e}\int_{h/2}^{h/2+h_P} z_P\,\mathrm{d}z + \frac{1}{R}e_{24e}\int_{h/2}^{h/2+h_P}\frac{P(z_P)}{R+z}\,\mathrm{d}z\frac{\partial^2}{\partial \theta^2} + e_{15e}\int_{h/2}^{h/2+h_P} P(z_P)\,\mathrm{d}z\frac{\partial^2}{\partial x^2}$$

$$L_{41}=\bar{B}_{11}\frac{\partial^2}{\partial x^2}+\frac{\bar{B}_{66}}{R^2}\frac{\partial^2}{\partial\theta^2},\quad L_{42}=\frac{\bar{B}_{12}+\bar{B}_{66}}{R}\frac{\partial^2}{\partial x\,\partial\theta},\quad L_{43}=\left(\frac{\bar{B}_{12}}{R}-\bar{C}_{44}\right)\frac{\partial}{\partial x}$$

$$L_{44}=\bar{D}_{11}\frac{\partial^2}{\partial x^2}+\frac{\bar{D}_{66}}{R^2}\frac{\partial^2}{\partial\theta^2}-\bar{C}_{44},\quad L_{45}=\frac{\bar{D}_{12}+\bar{D}_{66}}{R}\frac{\partial^2}{\partial x\,\partial\theta}$$

$$L_{46}=\left(2e_{31e}\int_{h/2}^{h/2+h_P}zz_P\,\mathrm{d}z-e_{15e}\int_{h/2}^{h/2+h_P}P(z_P)\,\mathrm{d}z\right)\frac{\partial}{\partial x}$$

$$L_{51}=\frac{\bar{B}_{66}+\bar{B}_{12}}{R}\frac{\partial^2}{\partial x\,\partial\theta},\quad L_{52}=\bar{B}_{66}\frac{\partial^2}{\partial x^2}+\frac{\bar{B}_{22}}{R^2}\frac{\partial^2}{\partial\theta^2}+\frac{\bar{C}_{55}}{R},\quad L_{53}=\frac{\bar{B}_{22}-\bar{C}_{55}R}{R^2}\frac{\partial}{\partial\theta}$$

$$L_{54}=\frac{\bar{D}_{12}+\bar{D}_{66}}{R}\frac{\partial^2}{\partial x\,\partial\theta},\quad L_{55}=\frac{\bar{D}_{22}}{R^2}\frac{\partial^2}{\partial\theta^2}-\bar{C}_{55}+\bar{D}_{66}\frac{\partial^2}{\partial x^2}$$

$$L_{56}=\left[\frac{1}{R}2e_{32e}\int_{h/2}^{h/2+h_P}zz_P\,\mathrm{d}z-e_{24e}\int_{h/2}^{h/2+h_P}\frac{P(z_P)}{R+z}\,\mathrm{d}z\right]\frac{\partial}{\partial\theta}$$

$$L_{61}=\frac{e_{31e}}{R}h_P\frac{\partial}{\partial x},\quad L_{62}=\frac{e_{32e}h_P}{R^2}\frac{\partial}{\partial\theta},\quad L_{63}=e_{15e}h_P\frac{\partial^2}{\partial x^2}+\frac{e_{24e}h_P}{R^2}\frac{\partial^2}{\partial\theta^2}+\frac{e_{32e}h_P}{R^2}$$

$$L_{64}=\left(e_{15e}h_P+e_{31e}h_P+\frac{e_{31e}}{R}\int_{h/2}^{h/2+h_P}z\,\mathrm{d}z\right)\frac{\partial}{\partial x},\quad L_{65}=\left(\frac{e_{24}h_P}{R}+\frac{e_{32e}h_P}{R}+\frac{e_{32e}}{R^2}\int_{h/2}^{h/2+h_P}z\,\mathrm{d}z\right)\frac{\partial}{\partial\theta}$$

$$L_{66}=-\xi_{11e}\int_{h/2}^{h/2+h_P}P(z_P)\,\mathrm{d}z\frac{\partial^2}{\partial x^2}-\xi_{22e}\int_{h/2}^{h/2+h_P}\frac{P(z_P)}{R(R+z)}\,\mathrm{d}z\frac{\partial^2}{\partial\theta^2}-2\xi_{33e}h_P-\frac{2\xi_{33e}}{R}\int_{h/2}^{h/2+h_P}z_P\,\mathrm{d}z$$

$$a_1=-\int_{-h/2}^{h/2}[Q_{11}(z)+Q_{12}(z)]\alpha_{eff}(z)T(z)\,\mathrm{d}z-\int_{h/2}^{h/2+h_P}[Q_{11e}\alpha_{11e}+Q_{12e}\alpha_{22e}]T(z)\,\mathrm{d}z$$

$$a_2=-\frac{1}{R}\int_{-h/2}^{h/2}[Q_{12}(z)+Q_{22}(z)]\alpha_{eff}(z)T(z)\,\mathrm{d}z-\frac{1}{R}\int_{h/2}^{h/2+h_P}[Q_{12e}\alpha_{11e}+Q_{22e}\alpha_{22e}]T(z)\,\mathrm{d}z$$

$$a_3=\frac{1}{R}\int_{-h/2}^{h/2}[Q_{12}(z)+Q_{22}(z)]\alpha_{eff}(z)T(z)\,\mathrm{d}z+\frac{1}{R}\int_{h/2}^{h/2+h_P}[Q_{12e}\alpha_{11e}+Q_{22e}\alpha_{22e}]T(z)\,\mathrm{d}z$$

$$a_4=-\int_{-h/2}^{h/2}[Q_{11}(z)+Q_{12}(z)]\alpha_{eff}(z)T(z)z\,\mathrm{d}z-\int_{h/2}^{h/2+h_P}[Q_{11e}\alpha_{11e}+Q_{12e}\alpha_{22e}]T(z)z\,\mathrm{d}z$$

$$a_5=-\frac{1}{R}\int_{-h/2}^{h/2}[Q_{12}(z)+Q_{22}(z)]\alpha_{eff}(z)T(z)z\,\mathrm{d}z-\frac{1}{R}\int_{h/2}^{h/2+h_P}[Q_{12e}\alpha_{11e}+Q_{22e}\alpha_{22e}]T(z)z\,\mathrm{d}z$$

$$a_{61}=\int_{h/2}^{h/2+h_P}T(z)p_{xe}\,\mathrm{d}z,\quad a_{62}=\frac{1}{R}\int_{h/2}^{h/2+h_P}T(z)p_{\theta e}\,\mathrm{d}z,\quad a_{63}=\int_{h/2}^{h/2+h_P}T'(z)p_{ze}\,\mathrm{d}z+\frac{1}{R}\int_{h/2}^{h/2+h_P}T(z)p_{ze}\,\mathrm{d}z$$

References

[1] V. Giurgiutiu, A.N. Zagrai, J. Bao, Damage identification in aging aircraft structures with piezoelectric wafer active sensors, *Journal of Intelligent Material Systems and Structures* 15 (2004) 673–687.

[2] Y.W. Yang, S. Bhalla, C. Wang, C.K. Soh, J. Zhao, Monitoring of rocks using smart sensors, *Tunnelling and Underground Space Technology* 22 (2006) 206–221.
[3] Y.W. Yang, J.F. Xu, C.K. Soh, Generic impedance-based model for structure—piezoceramic interacting system, *Journal of Aerospace Engineering* 18 (2005) 93–101.
[4] Y.W. Yang, Y.H. Hu, Electromechanical impedance modeling of PZT transducers for health monitoring of cylindrical shell structures, *Smart Materials and Structures* 17 (2008) 1–11.
[5] P. Heyliger, S. Brooks, Free-vibration of piezoelectric laminates in cylindrical bending, *International Journal of Solids and Structures* 32 (1995) 2945–2960.
[6] P. Heyliger, D.A. Saravanos, Exact free-vibration analysis of laminated plates with embedded piezoelectric layers, *Journal of the Acoustic Society of America* 98 (1995) 1547–1557.
[7] M. D'Ottavio, D. Ballhause, B. Kröplin, E. Carrera, Closed-form solutions for the free-vibration problem of multilayered piezoelectric shells, *Computers and Structures* 84 (2006) 1506–1518.
[8] S.S. Vel, B.P. Baillargeon, Analysis of static deformation, vibration and active damping of cylindrical composite shells with piezoelectric shear actuators, *Journal of Vibration and Acoustics* 127 (2005) 395–407.
[9] H.S. Tzou, Y.A. Bao, Theory on anisotropic piezothermoelastic shell laminates with sensor/actuator applications, *Journal of Sound and Vibration* 184 (1995) 453–473.
[10] H.S. Tzou, R. Ye, Piezothermoelasticity and precision control of piezoelectric systems: theory and finite element analysis, *Journal of Vibration and Acoustics* 116 (1994) 489–495.
[11] J.N. Reddy, C.D. Chin, Thermomechanical analysis of functionally graded cylinders and plates, *Journal of Thermal Stresses* 26 (1998) 593–626.
[12] J.N. Reddy, Analysis of functionally graded plates, *International Journal for Numerical Methods in Engineering* 47 (2000) 663–684.
[13] E. Carrera, S. Brischetto, A. Robaldo, Variable kinematic model for the analysis of functionally graded material plates, *AIAA Journal* 46 (2008) 194–203.
[14] S. Brischetto, R. Leetsch, E. Carrera, T. Wallmersperger, B. Kröplin, Thermo-mechanical bending of functionally graded plates, *Journal of Thermal Stresses* 31 (2008) 286–308.
[15] B. Mirzavand, M.R. Eslami, Thermal buckling of simply supported piezoelectric FGM cylindrical shells, *Journal of Thermal Stresses* 30 (2007) 1117–1135.
[16] X.Q. He, T.Y. Ng, S. Sivashanker, K.M. Liew, Active control of FGM plates with integrated piezoelectric sensors and actuators, *International Journal of Solids and Structures* 38 (2001) 1641–1655.
[17] T.Y. Ng, X.Q. He, K.M. Liew, Finite element modeling of active control of functionally graded shells in frequency domain via piezoelectric sensors and actuators, *Computational Mechanics* 28 (2002) 1–9.
[18] K.M. Liew, X.Q. He, T.Y. Ng, S. Sivashanker, Active control of FGM plates subjected to a temperature gradient; modelling via finite element method based on FSDT, *International Journal for Numerical Methods in Engineering* 52 (2001) 1253–1271.
[19] K.M. Liew, X.Q. He, T.Y. Ng, S. Kitipornchai, Active control of FGM shells subjected to a temperature gradient via piezoelectric sensor/actuator patches, *International Journal for Numerical Methods in Engineering* 55 (2002) 653–668.
[20] L. Fryba, Vibration of Solids and Structures Under Moving Loads, Noordhoff International, Groningen, The Netherlands, 1977.
[21] S.S. Law, Y.L. Fang, Moving force identification: optimal state estimation approach, *Journal of Sound and Vibration* 239 (2001) 233–254.
[22] X.Q. Zhu, S.S. Law, J.Q. Bu, A state space formulation for moving loads identification, *Journal of Vibration and Acoustics* 128 (2006) 509–520.
[23] X.Q. Zhu, S.S. Law, Dynamic behavior of orthotropic rectangular plates under moving loads, *Journal of Engineering Mechanics* 129 (2003) 79–87.
[24] S.S. Law, J.Q. Bu, X.Q. Zhu, S.L. Chan, Moving load identification on a simply supported orthotropic plate, *International Journal of Mechanical Sciences* 49 (2007) 1262–1275.
[25] V.A. Krysko, J. Awrejcewicz, A.N. Kutsemako, K. Broughan, Interaction between flexible shells (plates) and a moving lumped body, *Communications in Nonlinear Science and Numerical Simulation* 11 (2006) 13–43.
[26] M. Ruzzene, A. Baz, Dynamic stability of periodic shells with moving loads, *Journal of Sound and Vibration* 296 (2006) 830–844.
[27] R. Kadoli, N. Ganesan, Buckling and free vibration analysis of functionally graded cylindrical shells subjected to a temperature-specified boundary condition, *Journal of Sound and Vibration* 289 (2006) 450–480.
[28] J.N. Reddy, *Mechanics of Laminated Composite Plates and Shells*, second ed., CRC Press, New York, 2004.
[29] A. Fernandes, J. Pouget, Structural response of composite plates equipped with piezoelectric actuators, *Computers and Structures* 84 (2006) 1459–1470.
[30] J.D. Yau, L. Fryba, Response of suspended beams due to moving loads and vertical seismic ground excitations, *Engineering Structures* 29 (2007) 3255–3262.
[31] C.W. Lim, Y.F. Ma, S. Kitipornchai, C.M. Wang, R.K.K. Yuen, Buckling of vertical cylindrical shells under combined end pressure and body force, *Journal of Engineering Mechanics* 129 (2003) 876–884.
[32] Y.W. Kim, Temperature dependent vibration analysis of functionally graded rectangular plates, *Journal of Sound and Vibration* 284 (2005) 531–549.
[33] F. Ramirez, P.R. Heyliger, E. Pan, Free vibration response of two-dimensional magneto–electro-elastic laminated plates, *Journal of Sound and Vibration* 292 (2006) 626–644.

[34] N. Ganesan, R. Kadoli, Semianalytical finite element analysis of piezothermoelastic shells of revolution, *Computers and Structures* 83 (2005) 1305–1319.
[35] S.P. Timoshenko, J.M. Gere, *Theory of Elastic Stability*, McGraw-Hill, New York, 1961.
[36] H.R. Radwan, J. Genin, Dynamic instability in cylindrical shells, *Journal of Sound and Vibration* 56 (1978) 373–382.
[37] T.Y. Ng, K.M. Lam, K.M. Liew, J.N. Reddy, Dynamic stability analysis of functionally graded cylindrical shells under periodic axial loading, *International Journal of Solids and Structures* 38 (2001) 1295–1309.